# Early time diffusion for the quantum kicked rotor with narrow initial momentum distributions

A. J. Daley* and A. S. Parkins
*Department of Physics, University of Auckland, Private Bag 92019, Auckland, New Zealand*
(Received 27 June 2002; published 26 November 2002)

We investigate analytically and numerically early-time momentum diffusion rates for the $\delta$-kicked rotor across the quantum to classical transition, i.e., as increased total system action produces more macroscopic dynamics. For sufficiently narrow initial momentum distributions we find a rich structure of resonances in these diffusion rates as a function of the effective Planck's constant. Our study is set in the physical context of the atom optics kicked rotor, and numerical simulations confirm that the resonances persist with kicks of finite duration and with other typical experimental imperfections, such as spontaneous emission noise. Our results should be testable in experiments where narrow initial momentum distributions are prepared using, for example, velocity selective Raman transitions or Bose-Einstein condensates.

DOI: 10.1103/PhysRevE.66.056210 PACS number(s): 05.45.Mt, 03.65.Yz, 42.50.Lc

## I. INTRODUCTION

In recent years there has been much interest in studying the transition from quantum to classical behavior in the $\delta$-kicked rotor (DKR), as an example of a nonlinear dynamical system which exhibits contrasting behavior in the two regimes. In particular, the chaotic diffusion in the classical DKR is completely suppressed by coherence effects in the analogous quantum system [1,2]. This phenomenon, known as dynamical localization, has been demonstrated, along with many other properties of the DKR, in atom optics experiments in which a cloud of laser-cooled atoms interacts with a pulsed standing wave of light [3]. In these experiments, the DKR must be generalized to kicks of finite length, and the resulting system is referred to simply as the kicked rotor.

Recently there have been several studies of resonance phenomena in the diffusion rates for the DKR as the dynamics of the system are made more macroscopic or less macroscopic by varying the total system action, i.e., by varying the effective Planck's constant for the system. These studies have focused largely on the diffusion rates found in the late-time regime when the process of dynamical localization is disturbed by a fixed level of decoherence. Decoherence produced by various forms of environmental coupling has been investigated, including continuous position measurements [4] and, specifically in the atom optics kicked rotor (AOKR), spontaneous emission decoherence [5]. The diffusion resonances found for spontaneous emission decoherence have also been verified in AOKR experiments [6–8].

Resonances are also known to occur in early-time momentum diffusion rates for the quantum DKR, that is, the diffusion rates after just a few kicks. These resonances appear in results derived by Shepelyansky [9], and have also been investigated numerically for the AOKR [5]. However, these studies have typically taken place in the context of a system with a relatively broad initial momentum distribution (e.g., for the AOKR in Ref. [5], with a thermal distribution corresponding to a temperature of around 10 $\mu$K). For such initial momentum distributions, the momentum diffusion rates for the first two kicks in the quantum and classical systems are equal, giving a short period of time over which quantum mechanical effects are essentially unimportant in determining the dynamics of the system.

However, recent experiments in quantum chaos using cold atoms in optical potentials have begun with much narrower initial momentum distributions, either by using Bose-Einstein condensates [10] or by selecting a slice of a thermal distribution using velocity selective Raman transitions [11]. In this article, we show that for a sufficiently narrow initial momentum distribution, a much richer structure of diffusion resonances in action space is observed than that predicted by the results of Shepelyansky. These resonances arise *even in the second kick*, for which we derive an exact result. We also use numerical simulations to investigate the corresponding resonances in kicks 3–5. These resonances are pronounced and should be observable experimentally; this is emphasized by our numerical simulations, which extend these results to a system with a finite pulse length and physically realistic levels of noise. Our analytical results are applicable generically to the quantum DKR, but we set our study in the context of the AOKR to emphasize that our results should be directly testable against experiments with cold atoms.

## II. THE SYSTEM

The AOKR is realized using a cloud of ultracold atoms which interact with a standing wave of laser light of frequency $\omega_l$, detuned far from the frequency $w_0$ of the appropriate atomic transition. The laser is pulsed with period $T$ and pulse profile $f(t)$. Due to the large detuning, the internal atomic dynamics can be eliminated, and the resulting single particle Hamiltonian (for just the external degrees of freedom) is [3]

$$\hat{H}=\frac{\hat{p}^2}{2m}-\frac{\hbar\Omega_{eff}}{8}\cos(2k_l\hat{x})\sum_{n=1}^{N} f(t-nT), \qquad (1)$$

where $\hat{x}$ and $\hat{p}$ are the atomic position and momentum operators, respectively, and $k_l$ is the wave number of the laser light. The effective potential strength is $\Omega_{eff}=\Omega^2/\delta$, where $\Omega/2$ is the resonant Rabi frequency, and $\delta$ is the detuning

*Present address: Institut für Theoretische Physik, Universität Innsbruck, A-6020 Innsbruck, Austria. Electronic address: adal025@phy.auckland.ac.nz

 

from resonance. These quantities may be adjusted to account for hyperfine levels in any particular atomic species (see, for example, Ref. [5]). We can rewrite this Hamiltonian in dimensionless units as

$$\hat{H}' = \frac{\hat{\rho}^2}{2} - k\cos\hat{\phi}\sum_{n=1}^{\infty} f(t'-n). \tag{2}$$

Here, $\hat{\phi} = 2k_l\hat{x}$, $\hat{\rho} = 2k_l T\hat{p}/m$, $t' = t/T$, and $\hat{H}' = (4k_l^2 T^2/m)\hat{H}$. The classical stochasticity parameter is given by $\kappa = \Omega_{eff}\omega_R T\tau_p$, where $\tau_p$ is the pulse length and $\omega_R = \hbar k_l^2/2m$. In laboratory experiments it is common to choose $f(t')$ to be a square pulse, i.e., $f(t') = 1$ for $0 < t' < \alpha$, where $\alpha = \tau_p/T$, in which case $k = \kappa/\alpha$. If we choose $f(t')$ to be $\delta(t')$, then this system reduces to the standard DKR, and $k = \kappa$.

In the case of the DKR, the evolution of the system in the Heisenberg picture is represented by the standard map,

$$\hat{\phi}_{n+1} = \hat{\phi}_n + \hat{\rho}_n, \tag{3a}$$

$$\hat{\rho}_{n+1} = \hat{\rho}_n + \kappa\sin(\hat{\phi}_{n+1}), \tag{3b}$$

where $\hat{\phi}_n = \hat{\phi}(t' = n)$ and $\hat{\rho}_n = \hat{\rho}(t' = n)$, with the values recorded immediately after the kick at $t' = n$. Note that there are multiple definitions of the standard map, and in this one the first kick occurs at $t' = 1$.

In the scaled units, we have $[\hat{\phi}, \hat{\rho}] = i\bar{k}$, with $\bar{k} = 8\omega_R T$. Thus the quantum nature of the system is reflected by an effective Planck's constant $\bar{k}$ which scales as we change the total action in the system by altering the pulse period $T$. Note that with reference to the effective Planck's constant we can rewrite the relationship between the scaled momentum units $\rho$ and unscaled momentum units $p$ as

$$p/(2\hbar k_l) = \rho/\bar{k}. \tag{4}$$

## III. BACKGROUND

We define the momentum diffusion rate to be the change in the kinetic energy from one kick to the next,

$$D(n) = \frac{\langle\hat{\rho}_n^2\rangle}{2} - \frac{\langle\hat{\rho}_{n-1}^2\rangle}{2}. \tag{5}$$

Some investigations of momentum diffusion rates in both the quantum and classical DKR systems have used an alternative definition,

$$\tilde{D}(n) = \frac{\langle(\hat{\rho}_n - \hat{\rho}_0)^2\rangle}{2} - \frac{\langle(\hat{\rho}_{n-1} - \hat{\rho}_0)^2\rangle}{2}. \tag{6}$$

For sufficiently narrow momentum distributions and high kick strengths, these two definitions are essentially equivalent. We choose the first definition because it represents the quantity which is directly measured in experimental studies.

The primary analytical investigation of early-time quantum diffusion rates in the DKR was made by Shepelyansky [9,12]. Using the alternative definition $\tilde{D}(n)$ for the diffusion rate and assuming a uniform distribution of initial conditions in position and momentum space, he estimated the quantum diffusion rate for small kick numbers by computing a series of quantum correlations. (These calculations are reproduced in more detail in Ref. [13], and the results are summarized in the Appendix.) Shepelyansky's results predict broad resonances in the early-time diffusion rates as a function of $\bar{k}$, in particular for kicks 3–5. The correlations he evaluated also lead to the conclusion that diffusion rates for the first two kicks, $D(1)$ and $D(2)$, should be equal, and should be the same as the diffusion rate in the classical system for these two kicks for all $\bar{k}$, i.e., $D(1) = D(2) = \kappa^2/4$ (see the Appendix). This has been verified numerically [5] in the context of the AOKR with a typical thermal initial momentum distribution at a temperature of 10 $\mu K$, which corresponds to a distribution with a Gaussian width in unscaled units ($p$) of $\sigma_p/(2\hbar k_l) = 4$.

However, to our knowledge, no one has previously looked in detail at the equivalent results with much narrower initial momentum distributions, despite the fact that such distributions are accessible experimentally. In fact, using Raman transitions, Steck *et al.* have isolated momentum distributions with widths as narrow as $\sigma_p/(2\hbar k_l) = 0.03$ [11]. Furthermore, for sufficiently small values of $\bar{k}$, the initial momentum distribution in scaled units becomes very narrow even for ordinary thermal distributions, because Eq. (4) leads to a scaling of the width of the initial momentum distribution with $\bar{k}$ of the form $\sigma_\rho = \bar{k}\sigma_p/(2\hbar k_l)$. For such momentum distributions Shepelyansky's assumptions of uniform initial conditions break down. As we will demonstrate in the remaining sections of this article, this leads to diffusion rates on short timescales, including $D(2)$, which exhibit considerably more structure than that predicted for the case considered by Shepelyansky.

## IV. ANALYTICAL RESULTS FOR THE SECOND KICK

We can evaluate the diffusion rate for the DKR in the second kick, $D(2)$, by expanding the definition in Eq. (5) using the quantum standard map given in Eq. (3). Specifically, we can write

$$\begin{aligned} D(2) &= \langle\hat{\rho}_2^2\rangle/2 - \langle\hat{\rho}_1^2\rangle/2 \\ &= \frac{\kappa^2}{2}\langle\sin^2(\hat{\phi}_2)\rangle + \frac{\kappa}{2}\langle\hat{\rho}_1\sin(\hat{\phi}_2) + \sin(\hat{\phi}_2)\hat{\rho}_1\rangle \\ &= \frac{\kappa^2}{2}\langle\sin^2(\hat{\rho}_1 + \hat{\phi}_1)\rangle + \frac{\kappa}{2}\langle\hat{\rho}_1\sin(\hat{\phi}_1 + \hat{\rho}_1) \\ &\quad + \sin(\hat{\phi}_1 + \hat{\rho}_1)\hat{\rho}_1\rangle. \end{aligned} \tag{7}$$

We first evaluate the expectation values for a single momentum eigenstate, $|\rho_0\rangle$, and then take an incoherent average over a Gaussian momentum distribution to obtain a final expression for $D(2)$. Evaluating the expectation values for the single momentum eigenstate is algebraically intensive, and

involves multiple applications of several identities. Most notably, we require two special cases of the Baker-Hausdorff relation, in particular,

$$e^{\hat{A}+\hat{B}} = e^{\hat{B}} e^{\hat{A}} e^{[\hat{A},\hat{B}]/2} \tag{8}$$

for $\hat{A}$ and $\hat{B}$ such that $[\hat{A},[\hat{A},\hat{B}]]=[\hat{B},[\hat{B},\hat{A}]]=0$, and

$$\exp(\hat{A}+\hat{B}) = \exp[\hat{B}(e^c-1)/c]\exp(\hat{A}), \tag{9}$$

for $\hat{A}$ and $\hat{B}$ such that $[\hat{A},\hat{B}]=c\hat{B}$, where $c$ is a constant. We also make use of the Bessel function identities

$$\cos[z\sin(\theta)] = J_0(z) + 2\sum_{k=1}^{\infty} J_{2k}(z)\cos(2k\theta)$$

and

$$\sin[z\sin(\theta)] = 2\sum_{k=0}^{\infty} J_{2k+1}(z)\sin[(2k+1)\theta],$$

where $J_\nu(z)$ is an ordinary Bessel function of order $\nu$.

This derivation is presented in detail in Ref. [14]. The expectation value for a single momentum eigenstate is found to be

$$\begin{aligned}\langle\rho_0|\hat{\rho}_2^2|\rho_0\rangle - \langle\rho_0|\hat{\rho}_1^2|\rho_0\rangle &= \frac{1}{2}\kappa^2[1-J_2(K_{2q})\cos(2\rho_0)] - 2\kappa J_1(K_q)\rho_0\sin(\rho_0) \\ &+ \kappa^2[J_0(K_q)-J_2(K_q)]\cos(\rho_0)\cos(\bar{k}/2),\end{aligned} \tag{10}$$

where $K_q = 2\kappa\sin(\bar{k}/2)/\bar{k}$ and $K_{2q} = 2\kappa\sin(\bar{k})/\bar{k}$. If we now average this over an incoherent Gaussian distribution of $\rho_0$ values which is centered on $\overline{\rho_0}$ and has width $\sigma_\rho$, we obtain the result

$$\begin{aligned}2D(2) = \frac{1}{2}\kappa^2[1-J_2(K_{2q})e^{-2\sigma_\rho^2}\cos(\overline{\rho_0})] - 2\kappa J_1(K_q) \\ \times[\sigma_\rho^2 e^{-\sigma_\rho^2/2}\cos(\overline{\rho_0}) + \overline{\rho_0} e^{-\sigma_\rho^2/2}\sin(\overline{\rho_0})] \\ + \kappa^2[J_0(K_q)-J_2(K_q)]\cos(\bar{k}/2)e^{-\sigma_\rho^2/2}\cos(\overline{\rho_0}).\end{aligned} \tag{11}$$

This is our final expression for the diffusion rate in the second kick, and we notice immediately that it reduces to the quasilinear value as the initial momentum distribution becomes broader, but it predicts complicated and interesting structure as a function of $\bar{k}$ for sufficiently small $\sigma_\rho$.

In the particular case where $\overline{\rho_0}=0$, we obtain the result

$$\begin{aligned}2D(2) = \frac{1}{2}\kappa^2(1-J_2(K_{2q})e^{-2\sigma_\rho^2}) - 2\kappa J_1(K_q)\sigma_\rho^2 e^{-\sigma_\rho^2/2} \\ + \kappa^2[J_0(K_q)-J_2(K_q)]\cos(\bar{k}/2)e^{-\sigma_\rho^2/2}.\end{aligned} \tag{12}$$

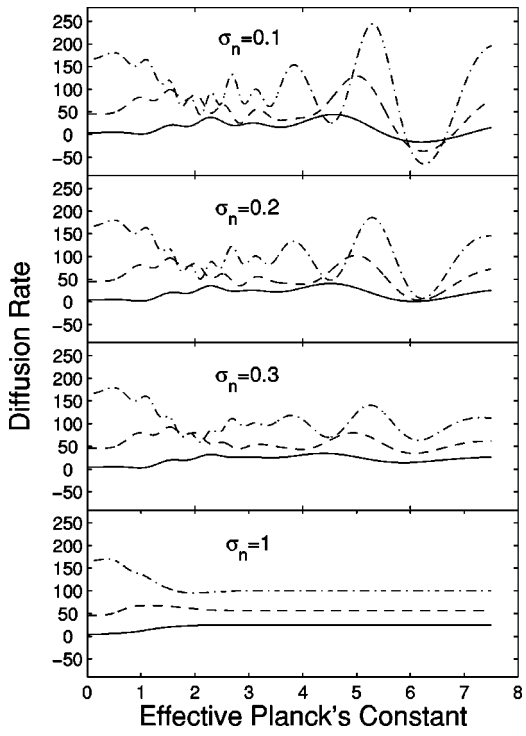


FIG. 1. Diffusion rates in the second kick, $D(2)$, for the quantum $\delta$-kicked rotor as a function of $\bar{k}$ plotted for various values of $\sigma_n = \sigma_p/(2\hbar k_l)$, with $\overline{\rho_0}=0$, as predicted by Eq. (12). Kick strengths are $\kappa=10$ (solid line), 15 (dashed line), and 20 (dash-dot line).

Fig. 1 shows Eq. (12) plotted as a function of $\bar{k}$ for three values of $\kappa$ and four values of $\sigma_n = \sigma_p/(2\hbar k_l)$ (i.e., $\sigma_\rho = \sigma_n\bar{k}$). We choose to vary the width of the initial momentum distribution in this way because in experiments using the AOKR, it is common to choose the initial temperature of the cloud, and then fix this value while $\bar{k}$ is varied. This corresponds to a fixed width in real momentum units, and hence a varying width in our scaled units. We see, as we expect, that for large values of $\sigma_n$, the diffusion rate is quasilinear except at low values of $\bar{k}$, where it tends to the diffusion rate for a single initial eigenstate, $|\rho_0=0\rangle$, as $\bar{k}\to 0$ and $\sigma_\rho\to 0$. For lower values of $\sigma_n$, we see a complicated resonance structure as a function of $\bar{k}$. This structure is a specifically quantum mechanical effect, because it relies on the $\bar{k}$ dependence of the correlations. It is particularly surprising that such a dramatic quantum effect can occur after only two kicks, and it is interesting that the structure is very different to that predicted by Shepelyansky. Moreover, we see from the $\sigma_n$ values in the figure that the initial momentum distributions which produce this structure should be experimentally realizable, as momentum distributions with $\sigma_n < 0.1$ can be produced using velocity selective Raman transitions, as demonstrated in Ref. [11], and using Bose-Einstein condensates [10].

We note that as the kick strength $\kappa$ is increased, the resonance peaks shift to higher $\bar{k}$ values, and increase in magnitude. Extra structure is also introduced at low $\bar{k}$ values for

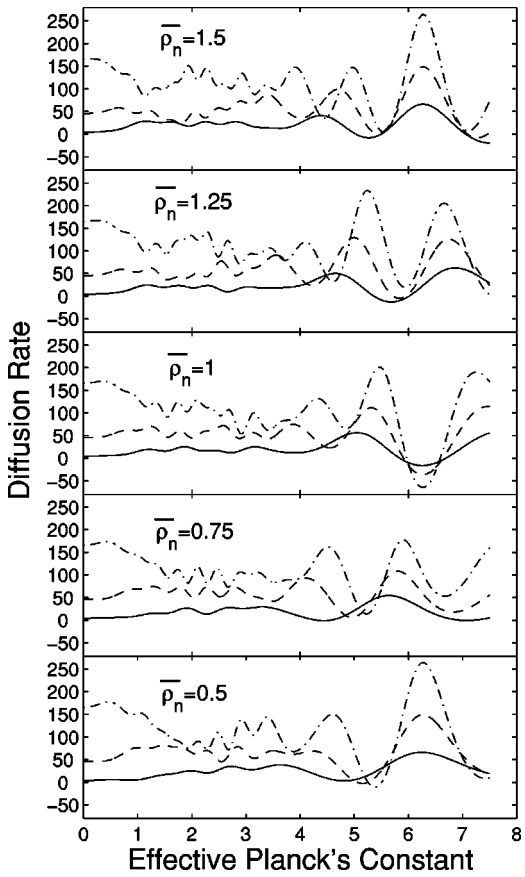


FIG. 2. Diffusion rates in the second kick, $D(2)$, for the quantum $\delta$-kicked rotor with $\sigma_n=0.1$, plotted as a function of $k$ for various values of $\overline{\rho_n}=\overline{p_0/(2\hbar k_l)}$, as predicted by Eq. (11). Kick strengths are $\kappa=10$ (solid line), 15 (dashed line), 20 (dash-dot line).

larger $\kappa$. This introduction of new structure continues to occur even for $\kappa$ values much larger than 20.

It is interesting to investigate how the resonance structure in the diffusion rate during the second kick changes if the initial momentum distribution is not centered on $\overline{\rho_0}=0$. Eq. (11) is plotted in Fig. 2 for various values of $\overline{\rho_n}=\overline{\rho_0/\bar{k}}=\overline{p_0/(2\hbar k_l)}$, with $\sigma_n=0.1$. As with the diffusion rates for $\overline{\rho_0}=0$, these rates exhibit interesting structure, which is washed out for large $\sigma_n$. This washing out can be seen from the dependence of Eq. (11) on the width of the initial momentum distribution. The most interesting feature here is that the positions of the diffusion rate resonances are strongly dependent on the value of $\overline{\rho_n}$. This is partly because different values of $\overline{\rho_0}$ give different weighting to different terms in the diffusion rate expression, but much of the variation results from the $\bar{k}$ dependence of $\overline{\rho_0}$ that occurs due to the scaling of our momentum units. Again, because it is possible to create initial momentum distributions with nonzero mean momentum with respect to the standing wave axis (see, for example, reference [11]), the initial momentum distributions which lead to these results should be experimentally realizable.

Another perspective on the variation of $D(2)$ as a function of $\kappa$, $\bar{k}$, and $\overline{\rho_n}$ is provided by Figs. 3–5. These figures show surface plots of $D(2)$ as a function of both $\kappa$ and $\bar{k}$ for

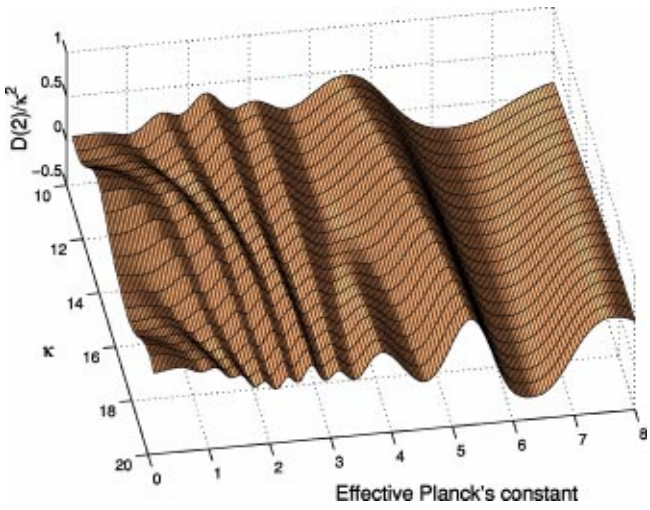


FIG. 3. Surface plot of $D(2)/\kappa^2$, for the quantum $\delta$-kicked rotor with an initial momentum eigenstate, $\rho_n=0$, as a function of $\bar{k}$ and $\kappa$, as predicted by Eq. (11).

three different initial momentum eigenstates, $|\rho_0=0\rangle$, $|\rho_0=0.5\bar{k}\rangle$, and $|\rho_0=\bar{k}\rangle$ (i.e., $\rho_n=0$, 0.5, and 1.0). Note that the diffusion rates have been divided by $\kappa^2$ so as to emphasize the positions of the diffusion resonances, rather than the increase in the rates as $\kappa$ becomes larger. Note also that the plots in Figs. 3–5 change only slightly if we consider an initial distribution of momenta, provided the width of this distribution $\sigma_n<0.1$. This is actually apparent from a comparison with corresponding curves in Figs. 1 and 2.

It is interesting to examine the relationship between the resonance structure observed here and so-called ''quantum resonances,'' which have been the subject of numerous investigations, such as the original treatments in Refs. [15–17] and the more recent analysis in Refs. [18,19]. Quantum resonances occur for particular values of $\bar{k}$, given appropriate initial conditions. For example, consider an initial momen-

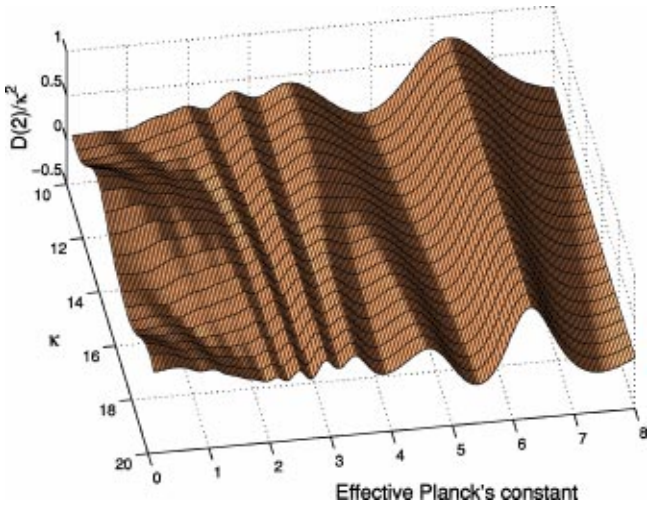


FIG. 4. Surface plot of $D(2)/\kappa^2$, for the quantum $\delta$-kicked rotor with an initial momentum eigenstate, $\rho_n=0.5$, as a function of $\bar{k}$ and $\kappa$, as predicted by Eq. (11).

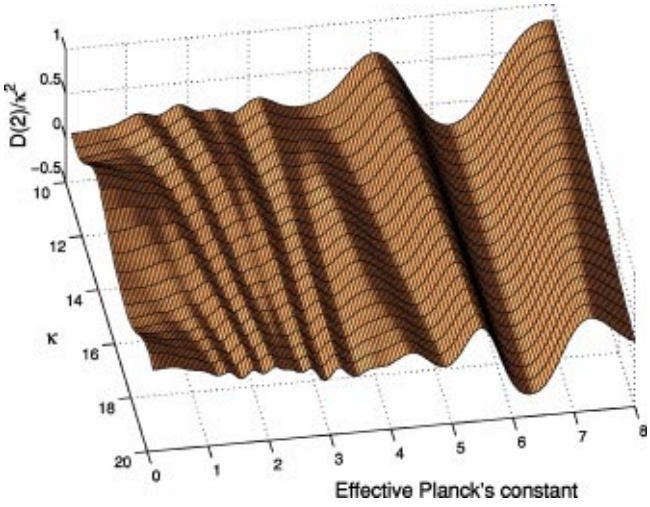


FIG. 5. Surface plot of $D(2)/\kappa^2$, for the quantum $\delta$-kicked rotor with an initial momentum eigenstate, $\rho_n=1$, as a function of $k$ and $\kappa$, as predicted by Eq. (11).

tum eigenstate $|\rho_0=j\hbar\rangle$, where $j$ is an integer. Through the kicking process, this state can only couple to eigenstates $|\rho=(j+j')\hbar\rangle$, where $j'$ is also an integer. If $\hbar$ is an even multiple of $2\pi$, then in between kicks the states $|\rho=(j+j')\hbar\rangle$ each accumulate the same phase (due to the free evolution operator $\exp[i\hat{\rho}^2/(2\hbar)]$), which is identically one. This leads to a ballistic energy growth, and dynamical localization does not occur.

In contrast, if $\hbar$ is an odd multiple of $2\pi$, then the phase may be either $+1$ or $-1$, and one finds, quite remarkably, that the system returns identically to its initial state after every second kick [16]. This effect is known as a ''quantum antiresonance,'' and shows up in Fig. 3 ($\rho_0=0$) and Fig. 5 ($\rho_0=\hbar$) as a minimum in $D(2)/\kappa^2$ at $\hbar=2\pi$ (with value $D(2)=-\kappa^2/4$, which cancels $D(1)=\kappa^2/4$ and returns the system to its initial energy).

Conversely, for $\rho_0=0.5\hbar$ (Fig. 4) we observe a maximum in $D(2)$ at $\hbar=2\pi$. This occurs because for all states with momenta $\rho=(j'+1/2)\hbar$, with $j'$ an integer, the accumulated phase between kicks is $(1+i)/\sqrt{2}$, i.e., the same. This leads to ballistic growth, with $D(2)=3\kappa^2/4$, or, in terms of energies, $E(n)=n^2\kappa^2/4+E(0)$.

The other resonances observed in these diffusion rates (i.e., those not occurring at $\hbar=2j\pi$ for integer $j$), are undoubtedly related to similar interference effects as those that cause ballistic motion at quantum resonances. This relationship could be very interesting, and deserves further investigation. However, the resonances we observe here are not solely the result of a simplification of the action of the free evolution operator on appropriate momentum eigenstates, as we observe at quantum resonances. Instead, they exhibit a nontrivial dependence on the value of $\kappa$, and appear to involve a complicated interaction between the particular momentum states that the system couples to during the first kick and the phase factors that those states accumulate during free evolution. This is illustrated by the dependence of the location of these maxima on both $\kappa$ and $\hbar$ in Figs. 3–5. In addition, many diffusion resonances occur at values of $\hbar$ for which we observe no clear periodic behavior as $\rho_n$ is varied. Such behavior should be a characteristic of ''regular'' quantum resonances.

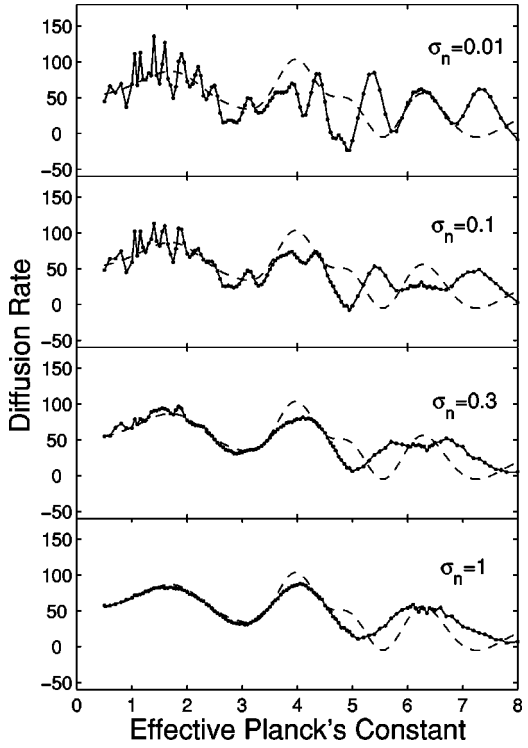


FIG. 6. Comparison of simulated diffusion rates in the third kick, $D(3)$, for the quantum kicked rotor ($\alpha=0.005$, $\eta=10\%$, $\kappa=15$, $\overline{\rho_0=0}$) with Shepelyansky's analytical result [Eq. (A5)], for varying values of $\sigma_n=\sigma_p/(2\hbar k_l)$. The simulation results are shown as points joined by a solid line, and the statistical errors in the points are approximately the same order of magnitude as the point markers. Shepelyansky's result is shown as a dashed line.

## V. NUMERICAL RESULTS FOR KICKS 3–5

To investigate similar results for kicks 3–5 we use numerical simulations, as exact analytical results for $D(n\geqslant 3)$ are complicated to obtain and because of their complexity would not significantly increase our understanding of the system. These simulations are set in the context of the AOKR, and model a master equation which includes effects due to spontaneous emission decoherence, the level of which is characterized by the position averaged spontaneous emission probability per kick, $\eta$. Our simulations are based on a Monte Carlo wave function method, as described in Refs. [5,20]. We typically use 1000 trajectories, sampled from the appropriate initial momentum distribution, and after evolving each of the trajectories we take an incoherent average over the final momentum distributions.

Figures 6, 7, and 8 show the diffusion rates $D(3)$, $D(4)$, and $D(5)$, respectively, and the early-time quantum diffusion rate predicted by Shepelyansky, Eq. (A5) is shown as a dotted line for comparison. It can be clearly seen that the

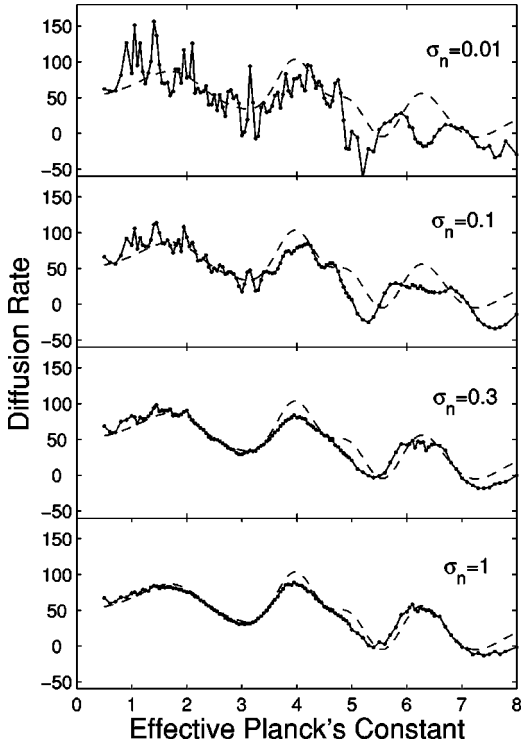


FIG. 7. Comparison of simulated diffusion rates in the fourth kick, $D(4)$, for the quantum kicked rotor ($\alpha=0.005$, $\eta=10\%$, $\kappa=15$, $\overline{\rho_0=0}$) with Shepelyansky's analytical result [Eq. (A5)], for varying values of $\sigma_n=\sigma_p/(2\hbar k_l)$. The simulation results are shown as points joined by a solid line, and the statistical errors in the points are approximately the same order of magnitude as the point markers. Shepelyansky's result is shown as a dashed line.

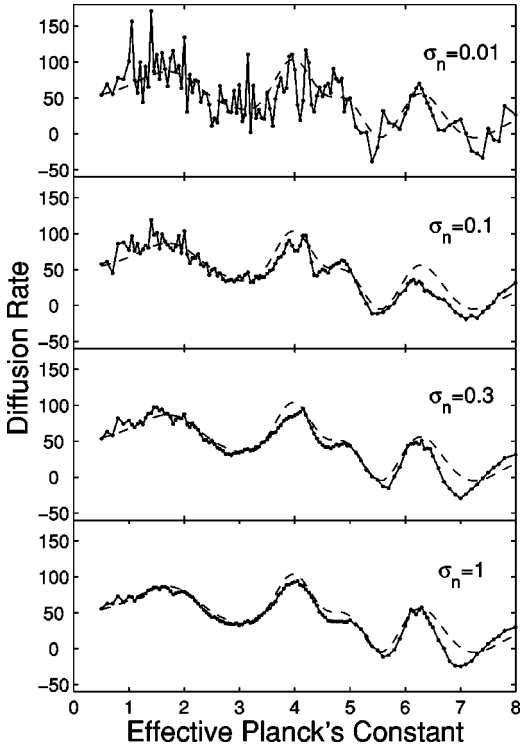


FIG. 8. Comparison of simulated diffusion rates in the fifth kick, $D(5)$, for the quantum kicked rotor (QKR) ($\alpha=0.005$, $\eta=10\%$, $\kappa=15$,$\overline{\rho_0=0}$) with Shepelyansky's analytical result [Eq. (A5)], for varying values of $\sigma_n=\sigma_p/(2\hbar k_l)$. The simulation results are shown as points joined by a solid line, and the statistical errors in the points are approximately the same order of magnitude as the point markers. Shepelyansky's result is shown as a dashed line.

system generally settles into a diffusion regime with rates similar to Shepelyansky's values as the kick number increases. However, we see a significant contrast in this behavior for different values of $\sigma_n$. Essentially, the broader the initial momentum distribution, the more rapidly the system settles into this regime. The lower the value of $\sigma_n$, the more complicated structure (and thus the least agreement with Shepelyansky's results) we observe in the diffusion rates. The most complex structure normally occurs at low values of $\bar{k}$, where the scaling of the initial momentum distribution for the AOKR makes the distribution the most narrow.

It is interesting to note, for $\sigma_n=0.01$, the behavior of the maxima and minima at $\bar{k}=2\pi$ due to the quantum antiresonance. As we expect, we observe a maximum at this point for the diffusion rate in the third kick, but we observe a minimum for the diffusion rate in the fourth kick (as the system with an initial momentum eigenstate $|\rho_0=0\rangle$ would return again to that initial eigenstate after every second kick). Even for such a narrow initial momentum distribution, however, the value at the minimum in the fourth kick is not as small as we would expect $(-\kappa^2/4)$ for an initial state $|\rho_0=0\rangle$, and the quantum resonance effects here are quite clearly washed out by a broader initial momentum distribution.

## VI. EXPERIMENTAL CONSIDERATIONS

In order to confirm that our results are experimentally measurable, we need to investigate these resonance structures in the context of a kicked rotor with a finite pulse length, and with the addition of noise sources commonly present in an AOKR. To do this we use the same numerical simulations described in the previous section. Example results from these simulations are presented in Fig. 9, along with the analytical results from Eq. (12). These two sets of results exhibit excellent quantitative agreement, as do simulation results for other values of $\kappa$ and $\sigma_n$. Similar simulations with an initial momentum distribution which is not centered on $\rho=0$ also exhibit very good agreement with the corresponding analytical results. This is very encouraging, and gives a strong indication that these results are realizable in a real experimental system.

We have also added other noise sources to our simulations such as amplitude noise on the kicking strength, which models variation in the intensity of the laser pulses producing the standing wave. In addition, we have accounted for a radial Gaussian intensity profile of the standing wave by including in our model a small spread of kick strengths equivalent to that across the cloud of atoms. With realistic levels of noise, we still observe resonances which are sufficiently pronounced to be experimentally measureable.

In a typical AOKR experiment, the initial cloud is released from an optical trap, the cloud is kicked using the pulsed standing wave, and is then allowed to expand freely for a certain period of time. The momentum distribution is

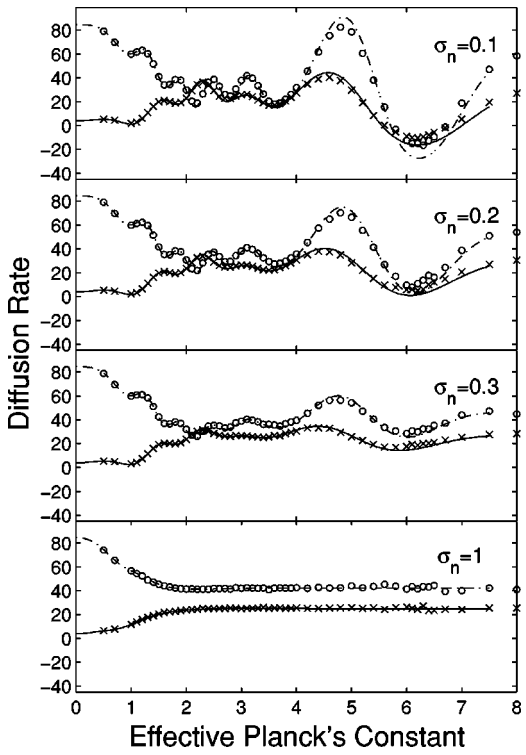


FIG. 9. Comparison of simulated diffusion rates in the second kick, $D(2)$, for the quantum kicked rotor ($\alpha=0.005$, $\eta=10\%$, $\overline{\rho_0}=0$) with analytical values predicted from Eq. (12). Kick strengths are $\kappa=10$ (solid lines and crosses) and 13 (dash-dot line and circles). The points mark the simulated values, and the lines mark analytical results.

inferred by imaging the final cloud after the free expansion period. Because of this, another possible concern for the experimental realizablility of our results is that with diffusion rates only being measured across two kicks, it may be difficult to resolve the resonance structures in the AOKR in terms of the width of the expanded cloud. However, calculations based on the initial cloud size and the expansion times used in typical experiments have shown that both the magnitude of the diffusion rates and the variation in the diffusion rates around the resonances are sufficiently large that this should not be a problem.

## VII. SUMMARY

Our results predict a rich structure of resonances as a function of the effective Planck's constant in the diffusion rate for the QKR with a sufficiently narrow initial momentum distribution. For the second kick we have derived a relatively simple, exact analytical result describing these resonances, and for higher kick numbers we observe related structures in numerical simulations. On short timescales, the resonances exhibit a more complicated structure than those predicted by Shepelyansky for a system with a broad initial momentum distribution, although our results agree with those of Shepelyansky in the appropriate limits. The spacing and position of the resonances change if the center of the initial momentum distribution is shifted, and in general they shift and scale as the kick strength $\kappa$ is varied. The exception to the shifting of the resonances are the maxima and minima observed at $\hbar=2n\pi$ for integer $n$, which are directly related to the phenomenon of quantum resonances which occur most strongly at these $\hbar$ values.

The quantities investigated are directly measurable, and, using numerical simulations, we have extended our results to a system with a finite pulse length and various noise sources which are common in AOKR systems. Our results should be realizable using current experimental techniques involving the AOKR, with initial momentum distributions prepared either using a Bose-Einstein condensate, or velocity selective Raman transitions.

## ACKNOWLEDGMENTS

The authors would like to thank Sze Tan, Rainer Leonhardt, Mark Sadgrove, and Maarten Hoogerland for interesting and useful discussions on this work, and Andrew Doherty for providing the computer source code of Ref. [20], which formed the basis for our simulations. This work was supported by a Grant (No. UOA016) from the Marsden Fund of the Royal Society of New Zealand.

## APPENDIX: SHEPELYANSKY'S RESULTS

In this appendix we summarize the results of Shepelyansky's calculations of quantum correlations which led to his predictions for the early-time diffusion rate in the QKR. These calculations come from references [9,12], and are reproduced in more detail in Ref. [13].

From the alternative definition of the momentum diffusion rate given in Eq. (6), we can express $\tilde{D}(n)$ as a sum over symmetrized correlation functions,

$$\tilde{D}(n)=\frac{\kappa^2}{2}\sum_{i=-n-1}^{n-1} C_q(i), \tag{A1}$$

where

$$C_q(i)=\frac{1}{2}\langle\psi_0|\sin\hat{\phi}_i\sin\hat{\phi}_0+\sin\hat{\phi}_0\sin\hat{\phi}_i|\psi_0\rangle. \tag{A2}$$

Under the assumption that the initial state $|\psi_0\rangle$ is approximately uniform over phase space, so that

$$\langle\psi_0|e^{im\hat{\phi}_0}e^{in\hat{\rho}_0}|\psi_0\rangle=\delta_{m,0}\delta_{n,0}, \tag{A3}$$

where $\delta_{i,j}$ denotes the Kronecker delta, Shepelyansky derived the following results:

$$C_q(0)=\frac{1}{2},$$

$$C_q(1)=0,$$

$$C_q(2)=\frac{J_2(K_q)}{2}, \tag{A4}$$

$$C_q(3)=\frac{J_3^2(K_q)-J_1^2(K_q)}{2},$$

$$C_q(4)=\frac{J_2^2(K_q)+O(K_q^{-3/2})}{2},$$

where $K_q=2\kappa\sin(\hbar/2)/\hbar$ and $O(K_q^{-3/2})$ denotes terms of the order of $K_q^{-3/2}$. From this, Shepelyansky estimated the early-time quantum diffusion rate to be

$$D_q\approx\tilde{D}(5)\approx\frac{\kappa^2}{2}\left(\frac{1}{2}-J_2(K_q)-J_1^2(K_q)+J_2^2(K_q)+J_3^2(K_q)\right). \tag{A5}$$

We can also see that under the assumption of uniform initial conditions we obtain $\tilde{D}(2)=(\kappa^2/2)\Sigma_{i=-1}^{1}C_q(i)=\kappa^2/4$, which is the same as the classical result, but in contrast with the result derived in this article for the case of a narrow initial momentum distribution.


[1] G. Casati, B. V. Chirikov, F. M. Izrailev, and J. Ford, in *Stochastic Behaviour in Classical and Quantum Hamiltonian Systems*, Lecture Notes in Physics Vol. 93, edited by G. Casati and J. Ford (Springer-Verlag, Berlin, 1979).

[2] B.V. Chirikov, F.M. Izrailev, and D.L. Shepelyansky, Sov. Sci. Rev. C **2**, 209 (1981).

[3] M.G. Raizen, Adv. At., Mol., Opt. Phys. **41**, 43 (1999).

[4] T. Bhattacharya, S. Habib, K. Jacobs, and K. Shizume, Phys. Rev. A **65**, 032115 (2002).

[5] A.J. Daley, A.S. Parkins, R. Leonhardt, and S.M. Tan, Phys. Rev. E **65**, 035201(R) (2002).

[6] M.B. d'Arcy, R.M. Godun, M.K. Oberthaler, D. Cassettari, and G.S. Summy, Phys. Rev. Lett. **87**, 074102 (2001).

[7] M.B. d'Arcy, R.M. Godun, M.K. Oberthaler, G.S. Summy, K. Burnett, and S.A. Gardiner, Phys. Rev. E **64**, 056233 (2001).

[8] M.E.K. Williams, M.P. Sadgrove, and R. Leonhardt (unpublished).

[9] D.L. Shepelyansky, Physica D **28**, 103 (1987).

[10] W.K. Hensinger, H. Häffner, A. Browaeys, N.R. Heckenberg, K. Helmerson, C. McKenzie, G.J. Milburn, W.D. Phillips, S.L. Rolston, H. Rubinsztein-Dunlop, and B. Upcroft, Nature (London) **412**, 52 (2001).

[11] D.A. Steck, W.H. Oskay, and M.G. Raizen, Science **293**, 274 (2001).

[12] D.L. Shepelyansky, Theor. Math. Phys. **49**, 925 (1982).

[13] D.A. Steck, Ph.D. thesis (Physics), University of Texas at Austin, Austin, TX, USA, 2001 (unpublished).

[14] A.J. Daley, M.Sc. thesis (Physics), University of Auckland, Auckland, New Zealand, 2002 (unpublished).

[15] F.M. Izrailev and D.L. Shepelyansky, Sov. Phys. Dokl. **24**, 996 (1979).

[16] F.M. Izrailev and D.L. Shepelyansky, Theor. Math. Phys. **43**, 553 (1980).

[17] G. Casati and I. Guarneri, Commun. Math. Phys. **95**, 121 (1984).

[18] W.H. Oskay, D.A. Steck, V. Milner, B.G. Klappauf, and M.G. Raizen, Opt. Commun. **179**, 137 (2000).

[19] V.V. Sokolov, O.V. Zhirov, D. Alonso, and G. Casati, Phys. Rev. Lett. **84**, 3566 (2000).

[20] A.C. Doherty, K.M.D. Vant, G.H. Ball, N. Christensen, and R. Leonhardt, J. Opt. B: Quantum Semiclassical Opt. **2**, 605 (2000).